Lidar-derived estimate and uncertainty of carbon sink in successional phases of woody encroachment

Temuulen Sankey,[1] Rupesh Shrestha,[2] Joel B. Sankey,[3,4] Stuart Hardegree,[5] and Eva Strand[6]

Received 28 January 2013; revised 28 May 2013; accepted 22 June 2013; published 29 August 2013.

[1] Woody encroachment is a globally occurring phenomenon that contributes to the global carbon sink. The magnitude of this contribution needs to be estimated at regional and local scales to address uncertainties present in the global- and continental-scale estimates, and guide regional policy and management in balancing restoration activities, including removal of woody plants, with greenhouse gas mitigation goals. The objective of this study was to estimate carbon stored in various successional phases of woody encroachment. Using lidar measurements of individual trees, we present high-resolution estimates of aboveground carbon storage in juniper woodlands. Segmentation analysis of lidar point cloud data identified a total of 60,628 juniper tree crowns across four watersheds. Tree heights, canopy cover, and density derived from lidar were strongly correlated with field measurements of 2613 juniper stems measured in 85 plots (30 × 30 m). Aboveground total biomass of individual trees was estimated using a regression model with lidar-derived height and crown area as predictors (Adj. $R^2 = 0.76$, $p < 0.001$, RMSE = 0.58 kg). The predicted mean aboveground woody carbon storage for the study area was 677 g/m^2. Uncertainty in carbon storage estimates was examined with a Monte Carlo approach that addressed major error sources. Ranges predicted with uncertainty analysis in the mean, individual tree, aboveground woody C, and associated standard deviation were 0.35 – 143.6 kg and 0.5 – 1.25 kg, respectively. Later successional phases of woody encroachment had, on average, twice the aboveground carbon relative to earlier phases. Woody encroachment might be more successfully managed and balanced with carbon storage goals by identifying priority areas in earlier phases of encroachment where intensive treatments are most effective.

Citation: Sankey, T., R. Shrestha, J. B. Sankey, S. Hardegree, and E. Strand (2013), Lidar-derived estimate and uncertainty of carbon sink in successional phases of woody encroachment, *J. Geophys. Res. Biogeosci.*, *118*, 1144–1155, doi:10.1002/jgrg.20088.

1. Introduction

1.1. Woody Encroachment

[2] Woody encroachment into grass and shrublands is a global phenomenon [*Archer*, 1999; *Mather*, 2000]. The distribution and density of woody plant genera of *Acacia*, *Juniperus*, *Larrea*, *Prosopis*, *Quercus*, and *Tamarisk* are currently increasing in the world's arid and semi-arid regions, which comprise approximately 40% of the terrestrial land surface and include many ecosystems at risk [*Archer*, 1999; *Strand et al*., 2008]. Woody encroachment can decrease understory vegetation cover and forage, increase soil erosion, alter soil fertility, and degrade wildlife habitat [*Miller et al*., 2000]. To combat these effects, intensive land treatments, including prescribed burning and cutting, are commonly performed. The consequences of both woody encroachment and intensive land treatments for terrestrial carbon (C) stocks are unclear.

[3] Woody encroachment may contribute significantly to the global C sink. In North America, woody encroachment has been estimated to contribute 18–34% [0.06–0.13 PgCyr^{-1} (1 Pg = 10^{15} g)) of the continental C sink [*Houghton et al*., 1999; *Pacala and Hurtt*, 2001; *Houghton*, 2003]. Large uncertainties exist in these global- and continental-scale estimates due to the coarse scale of the data and models [*Pan et al*., 2011]. Intensive land treatment activities can slow down or reverse the accumulation of C stocks that occurs with woody encroachment [*Cline et al*., 2010]. Intensive land treatments are often applied to targeted locations

[1]Research Assistant Professor, School of Earth Sciences and Environmental Sustainability, Northern Arizona University, Flagstaff, Arizona, USA.
[2]Postdoctoral Research Associate, Boise Center Aerospace Laboratory, Idaho State University, Boise, Idaho, USA.
[3]USGS Western Geographic Science Center, Flagstaff, Arizona, USA.
[4]Now at Grand Canyon Monitoring and Research Center, U.S. Geological, Survey, Flagstaff, Arizona, USA.
[5]USDA-ARS Northwest Watershed Research Center, Boise, Idaho, USA.
[6]Department of Rangeland Ecology and Management, University of Idaho, Moscow, Idaho, USA.

Corresponding author: T. Sankey, Laboratory of Landscape Ecology and Conservation Biology, School of Earth Sciences and Environmental Sustainability, Rm 223, ARD Building, 1298 S. Knoles Drive, Northern Arizona University, Flagstaff, AZ 86011, USA. (Temuulen.Sankey@nau.edu)

2169-8953/13/10.1002/jgrg.20088

Table 1. Juniper Encroachment Phases and Their Characteristics in Postsettlement Stands (Adopted From *Miller et al*., 2005)[a]

Encroachment Phases	Tree Canopy Cover (%)	Tree Density
Phase I (early stage)	<10%	up to 200 trees/ha (18/pixel)
Phase II (mid stage)	10–30%	200–780 trees/ha (18–70/pixel)
Phase III (late/closed stage)	>30%	>780 trees/ha (>70 trees/pixel)

[a]The estimates in brackets show conversions from hectares to 30 m pixels.

to optimize treatment effects. Regional and local management policies, however, do not take into account the spatial variability in woody C accumulation as it varies with successional phases of encroachment. Regional and local-scale (i.e., subcontinental) estimates of woody C accumulation should consider C storage and land treatment effects, but current models have a high degree of uncertainty in predicting the magnitude of carbon accumulation rates in these systems.

[4] The primary objective of this study was to estimate woody carbon storage in varying juniper encroachment phases using high-resolution, three-dimensional lidar data. To achieve this objective, we used a segmentation analysis of lidar point cloud data and estimated aboveground biomass and associated uncertainty of individual juniper trees in the South Mountain area, southwestern Idaho, USA. We also classified juniper encroachment phases based on lidar-derived and field-measured juniper tree height, density, and canopy cover and compared *Miller et al*. [2000] and *Miller et al*. [2005] canopy cover and density thresholds to determine which criteria best characterized successional phases of encroachment and priority areas for intensive management when using remote sensing data over large areas.

1.2. Juniper Encroachment in Western North America

[5] The spatial extent of pinyon-juniper woodlands, the third most common vegetation type in the USA [*Huang et al*., 2009], is documented to have increased by an order of magnitude since the mid-19th century [*Romme et al*., 2009]. Literature reviews indicate that reported increases in areal extent have ranged between 30 and 625% [*Romme et al*., 2009], while encroachment rates have varied between 0.4 and 4.5% per year [*Sankey and Germino*, 2008]. At regional scales, the mean pinyon-juniper woodland contribution to terrestrial C is estimated to be 5.2 MgC/ha ($1\,\mathrm{Mg} = 10^6\,\mathrm{g}$), while mean C accumulation associated with pinyon-juniper encroachment is estimated to be 3.3–10 $\mathrm{gCm^{-2}\,yr^{-1}}$ [*Strand et al*., 2008]. Estimates of C accumulation, however, have varied greatly from −0.11 to 0.22 $\mathrm{MgCha^{-1}\,yr^{-1}}$ due to the methods and scale of analysis [*Strand et al*., 2008; *Huang et al*., 2009; *Davies and Bates*, 2010]. Previous optical and multispectral remote-sensing approaches provide only a two-dimensional measurement of juniper cover change [e.g., *Strand et al*., 2008; *Huang et al*., 2009; *Davies and Bates*, 2010]. We present a new technique to estimate aboveground woody C storage using high-resolution, three-dimensional lidar measurements of individual juniper trees in western juniper [*Juniperus occidentalis*] communities.

[6] Lidar data are now increasingly used for rangeland applications [*Weltz et al*., 1994; *Ritchie et al*., 1995; *Rango et al*., 2000; *Streutker and Glenn*, 2006; *Mundt et al*., 2006; *Bork and Su*, 2007; *Riano et al*., 2007; *Su and Bork*, 2007; *Sankey et al*., 2010; *Sankey and Bond*, 2011]. Tree height and crown diameter can be measured directly from lidar data [e.g., *Hyyppa et al*., 2001; *Popescu et al*., 2003]. Lidar analyses generally involve establishing relationships between metrics describing lidar-derived height measurements and ground-based data [e.g., *Means et al*., 2000; *Næsset and Gobakken*, 2008]. The estimation of aboveground biomass relies on a strong relationship between the amount of foliage and the various tree components since foliage normally is the main element blocking laser pulses [*Næsset and Gobakken*, 2008]. In this study, we present an object-based tree crown delineation approach, with segmentation followed by local maxima to detect individual tree crowns and compute the metrics from the lidar points within each tree crown area. This approach of computing metrics directly from the lidar point cloud, rather than from an interpolated raster surface, might improve lidar-based tree biomass estimation.

[7] Lidar-derived individual tree characterization has important implications for both C stock estimates and prioritization of juniper treatment activities. Juniper encroachment occurs in distinct successional phases that are correlated with juniper tree age, density, canopy cover, and individual tree biomass [*Miller and Rose*, 1999]. *Miller et al*. [2005] identified three distinct successional phases during the process of juniper encroachment: Phase I where trees are present, but shrub and herbaceous species dominate; Phase II where trees codominate with shrubs and herbaceous species; and Phase III where trees are the dominant vegetation (Table 1). *Johnson and Miller* [2006] further modeled tree density within each of these phases or cover classes to help identify critical transition points (Table 1). Lidar data offer key advantages in estimating tree canopy cover and tree density per unit area over large spatial extent based on individual tree characterization. However, it is uncertain which variable and threshold derived from lidar remote sensing data better describe juniper encroachment phases.

[8] Lidar-based measurements can provide high-resolution estimates of tree cover, density, and height that could be used to estimate tree biomass, C accumulation rate, and amount as a function of encroachment phase [*Asner et al*., 2010; *Koch*, 2010; *Popescu*, 2007]. Such estimates might in turn be useful to guide treatment activities in conjunction with greenhouse gas mitigation goals. Juniper control treatments are most effective during the early phases of stand development. As juniper trees mature and canopy cover increases in encroached area, understory vegetation cover decreases [*Tausch et al*., 1981] leading to lack of fine fuels for surface fires and making rangeland restoration difficult [*Johnson and Miller*, 2006]. Once a stand reaches mid to late development phases, control treatments are no longer effective [*Miller et al*., 2000].

2. Methods

2.1. Study Area

[9] This study was conducted in four research watersheds in the South Mountain area of southwestern Idaho. These

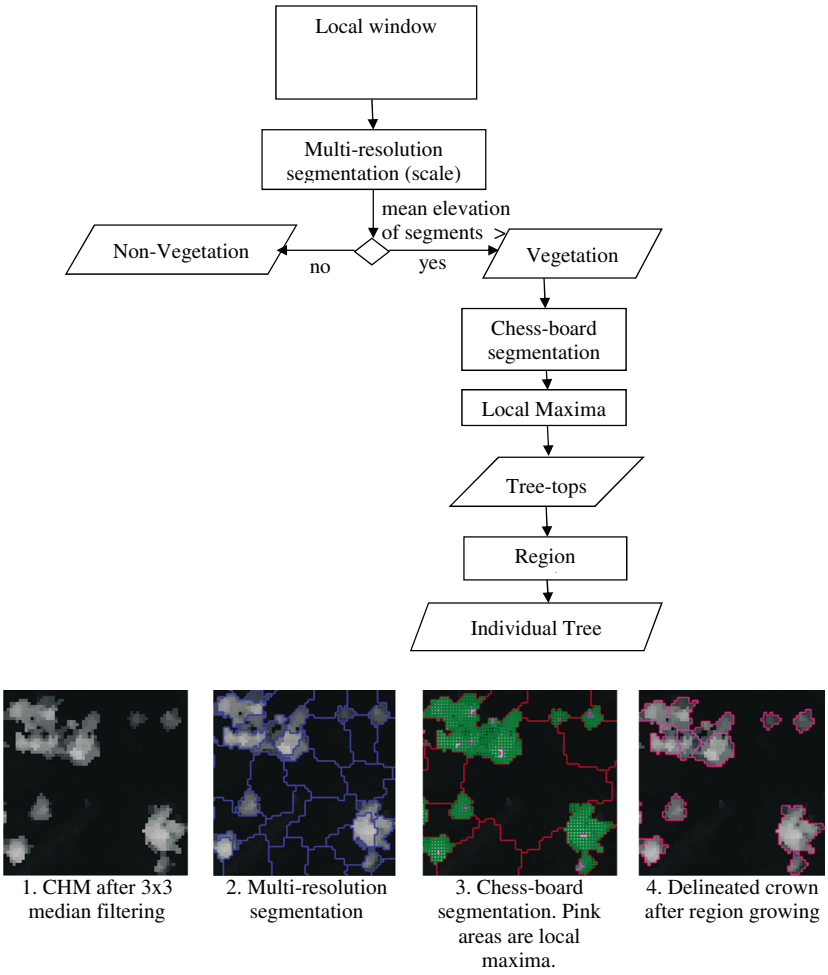

Figure 1. Individual tree crown delineation approach used in this study.

watersheds are part of a cooperative hydrology experiment by: USDA-ARS Northwest Watershed Research Center in Boise, ID; USDA-ARS Eastern Oregon Agricultural Experiment Station in Burns, OR; Idaho State University; the Bureau of Land Management; and private-land cooperators. The watersheds have been monitored for meteorological inputs, streamflow, and water quality parameters since October 2006. These watersheds range in size from 20 to 70 hectares adjacent to each other. Since all four watersheds share boundaries with similar encroachment phases, we treat them collectively as a study area. The study area would normally be occupied by mountain big sagebrush (*Artemesia tridentata* Nutt. spp. *vaseyana* [Rydb.] Beetle) with understory vegetation dominated by Idaho fescue (*Festuca idahoensis* Elmer) [*Bates et al*., 2011], but is encroached by western juniper (*Juniperus occidentalis*). No other tree species are found in the juniper stands.

2.2. Field Measurements

[10] Field work was completed in July–August 2010. A total of 100 random points were generated within the study area [Hawth's tools in ESRI® ArcMap 9.3 software: ESRI Inc, 1999–2006]. A 30 × 30 m Landsat image pixel at each of these random points was selected and the coordinates of the four corners of each pixel determined from the imagery. We established field plots by navigating to the four corners of the corresponding 30 × 30 m area on the ground [Trimble GeoXH GPS receiver: Trimble Navigation Ltd., Sunnyvale, California]. Within each field plot, every juniper stem was mapped, measured for height and canopy width, and classified as either mature tree (>2 m in height or >8 cm in diameter at 30 cm height) or seedling (<2 m in height or <8 cm in diameter at 30 cm height). Canopy width of individual trees was measured using the average of two line measurements perpendicular to each other and crossing at the tree trunk. Total tree canopy cover within each plot was estimated by adding canopy area measurements of all trees in the plot and dividing the sum by the area of the plot (900 m^2). Three mature trees closest to the center of each plot were cored at 30 cm height above ground with an increment borer to estimate juniper age. A total of 40 randomly selected seedlings were destructively sampled at ground height and 30 cm height to determine seedling age and to estimate an age-correction factor for older trees that were cored at 30 cm height.

2.3. Tree-Age Estimate

[11] Tree core samples were processed and dated using standard dendrochronological methods [*Stokes and Smiley*, 1968]. Only the samples that contained pith or samples that were geometrically estimated to have pith within five missing rings were selected for age estimates. A total of

Table 2. Candidate Individual Tree Metrics Used as Predictor Variables to Estimate Tree Biomass[a]

Statistics	All Returns	Canopy Returns	Ground Returns
Maximum height	H_{MAX}		
Minimum height	H_{MIN}	$H_{MIN}{}_C$	
Mean height	H_{MEAN}	$H_{MEAN}{}_C$	
Range of height	H_R	$H_R{}_C$	
Standard error of mean of height	H_{SE}	$H_{SE}{}_C$	
Sum of squares of height	H_{SS}	$H_{SS}{}_C$	
Quadratic mean of height	H_{QUAD}	$H_{QUAD}{}_C$	
Trimmed mean of height (mean after excluding 5% highest and 5% lowest values)	H_{TMEAN}	$H_{TMEAN}{}_C$	
Standard deviation of height	H_{STD}	$H_{STD}{}_C$	
Variance deviation of height	H_{VAR}	$H_{VAR}{}_C$	
Coefficient of variation of height	H_{CV}	$H_{CV}{}_C$	
Mean of squared successive difference	H_{MSSD}	$H_{MSSD}{}_C$	
x % Quantile of height (x =10, 25, 50, 75, 90)	H_{QX}	$H_{QX}{}_C$	
Interquartile range	H_{IQR}	$H_{IQR}{}_C$	
Skewness of height	H_{SKW}	$H_{SKW}{}_C$	H_{SKW}
Kurtosis of height	H_{KUR}	$H_{KUR}{}_C$	H_{KUR}
Total returns	N_T	N_C	N_G
Crown area		C_A	

[a]The final regression model included only two of these variables: crown area and sum of squares of vegetation height.

209 core samples (~90% of all samples) were dated successfully, and all seedling samples were successfully dated. The mean correction factor for tree age at 30 cm height was 10 years. Tree-age measurements were compared to field-measured tree height using a simple linear regression to evaluate uncertainties associated with tree ages estimated from lidar-derived juniper heights over large areas beyond the field plots.

2.4. Tree Biomass Estimate

[12] Aboveground biomass was estimated for the individual trees that were cored in the field. Basal circumference of each tree was calculated from increment core sample radius (e.g., distance from bark to pith). Biomass was estimated using allometric relationships between tree basal circumference and biomass of total foliage, live and dead branch, and stem wood and bark [*Gholz et al*., 1979]. These component biomass estimates were then added together to calculate total aboveground biomass of individual trees.

2.5. Lidar Data and Preprocessing

[13] The airborne lidar data were acquired in November 2007 through Watershed Sciences Inc. using a Leica ALS50 Phase II laser [Leica Geosystems AG, Heerbrugg, Switzerland] mounted on a Cessna Caravan 208B fixed wing aircraft flying at a 900 m height and an average 105 knot speed with 50% flightline overlap and a scan angle of ±14 degrees off nadir. The study area spanned four postprocessed lidar data tiles, which included a total of 11 original flightlines. The Leica ALS50 Phase II is a discrete return system that measures up to four laser returns per pulse. The lidar point cloud data had a maximum of four returns and mean point density of 5.6 points/m^2 with an average horizontal point spacing of approximately 17 cm. The mean horizontal relative and absolute accuracies were 32 cm and 33 cm, respectively, as reported by the vendor. The vertical accuracy was approximately 10 cm. Each point had the following attribute information: scan angle, return number, intensity, X, Y, and Z coordinates. The point cloud data were processed using previously described methods [*Streutker and Glenn*, 2006; http://bcal.geology.isu.edu/tools/lidar] to separate ground and vegetation returns. The vegetation point cloud data were first used to delineate individual juniper tree crowns and estimate individual juniper tree height and biomass. Next, the vegetation point cloud data were converted into a raster format to estimate total juniper tree density and canopy cover per unit area, which were then used as the two primary variables to classify juniper encroachment phases. The raster outputs were all produced in 30 × 30 m cells to compare with the field-based measurements in 30 × 30 m plots.

2.6. Lidar-Derived Juniper Crown Delineation

[14] The crowns of individual juniper trees were delineated using the lidar point cloud data via segmentation followed by a region-growing approach (Figure 1). eCognition software version 8.0 [Trimble Geospatial Inc., Colorado, USA] was used to perform a multiresolution segmentation of rasterized canopy height model (CHM) with 30 cm resolution. Multiresolution segmentation divides the CHM into groups of similar pixels using relative homogeneity criteria based on spectral value, shape, and texture of the features [*Benz et al*., 2004]. A scale parameter of 10, shape parameter of 0.1, and compactness value of 0.5 were used. The segments with multiple pixels and mean vegetation height >1 m were further divided into 30 cm squares, which were used to perform a variable window local maxima [*Popescu and Wynne*, 2004] to identify tree tops. Individual tree tops identified from local maxima were used as seed pixels for region growing to delineate individual tree crowns. The total area of lidar-delineated individual tree crown area was summed in 30 m cells (and divided by 900 m^2) and regressed with the total canopy diameter of all individual trees mapped in the 30 m plots (and divided by 900 m^2) via a linear regression.

2.7. Lidar-Derived Juniper Tree Biomass

[15] The lidar-delineated individual tree boundaries were overlaid on the lidar points and descriptive statistics computed for the distribution of lidar returns within each individual tree crown (Table 2). These descriptive statistics were regressed with estimated aboveground biomass. Once all significant variables were identified among the lidar descriptive statistics (Table 2), the best-subsets regression approach was used to select a parsimonious set of predictor variables to be included in the final model [Minitab version 16.1.1 software, Minitab Inc., Pennsylvania, USA]. Multicolinearity of all independent variables was tested using variance inflation factors (VIF) [*Hocking*, 2003]. If any of the variables had VIF value >10, then the variables with the highest VIF were removed, and the VIF was computed again with the new set of variables. This process was repeated until all the variables had VIF of ≤10. The best-subset regression was performed with the remaining independent variables that were significant ($\alpha = 0.05$). The preferred regression model was selected using the following criteria [*Montgomery et al*., 2006]: (1) maximum adjusted coefficient of determination (adj. R^2),

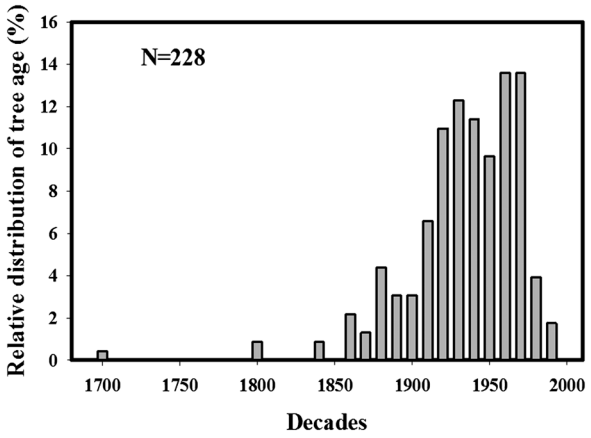

Figure 2. Western juniper tree-age distribution in South Mountain, Idaho, USA.

(2) minimum Mallows Cp, and (3) minimum mean square error. Models with fewer variables were preferred over larger models with slightly better values of adjusted R^2 or Cp. The predictive capability of the selected model was assessed using cross-validation multiple correlation [*Rozeboom*, 1978].

[16] Once the preferred regression model was identified, regression coefficients and lidar-derived variables were used to estimate the biomass of all trees delineated in the study area. Individual tree biomass was then converted to C by multiplying the weight by a factor of 0.5 following *Strand et al*. [2008], who estimated western juniper C content at a nearby site using aboveground tree biomass. The resulting individual tree C storage map was then overlaid with the encroachment phase map to estimate average aboveground C storage within each encroachment phase.

2.8. Tree Biomass Uncertainty Analysis

[17] We used a Monte Carlo approach adapted from *Gonzalez et al*. [2010] to quantify uncertainty in the biomass estimates. The approach estimated and propagated uncertainties for each major source and methodological step in the biomass calculations including field-based estimates, biomass regression estimates, lidar-derived estimates, and spatial autocorrelation [*Wang et al*., 2005; *Aalde et al*., 2006; *Gonzalez et al*., 2010].

[18] We performed 100 realizations of the field-based individual tree (n = 104) biomass allometric estimates. In the realizations, we incorporated error terms for the (1) field measurement errors of basal circumference and (2) statistical uncertainty of the tree allometric regression equations derived by *Gholz et al*. [1979]. We estimated the error term for the field measurement from the RMSE of the comparison of (i) basal circumference derived from basal diameter calculated (n = 95 trees) from the radius using the distance from bark to pith in a tree core sample versus (ii) basal circumference measured in the field. We estimated the error term for the allometric regression estimates from the standard error of regression for each allometric relationship in the component biomass estimates [reported in *Gholz et al*., 1979].

[19] For each set of tree biomass estimates derived from the outcome of the 100 realizations above, we regressed field-based individual tree (n = 104) biomass as a function of the VHSS and CA lidar variables, resulting in 100 regression equations. Following *Gonzalez et al*. [2010], we selected the coefficients and standard error of regression of the median of the 100 regression equations. The coefficients were used to estimate individual tree biomass for each tree (n = 60,628) identified by lidar analysis in the study area.

[20] Next, we performed 100 realizations of the biomass estimates incorporating error terms for (3) statistical uncertainty of the lidar variables and tree biomass relationship and (4) spatial autocorrelation. We estimated the error term for the lidar variables and tree biomass relationship from the standard error of regression of the median regression equation. Following *Gonzalez et al*. [2010], the error term for spatial autocorrelation was estimated from the standard error of the median regression scaled for each location by the absolute value of local Moran's *I* (measure of local spatial autocorrelation that ranges from negative- to no- to positive-correlation with possible values of −1 to 0 to 1, respectively).The local Moran's *I* was calculated for a one-cell lag from a raster of total biomass estimated in 30 m cells from the median regression equation and therefore identified the relative degree of local self-similarity across the continuum of spatially uniform to spatially random estimates. This resulted in 100 realizations of individual tree biomass for each tree identified by lidar in the study area. A mean and standard deviation for each tree was estimated from the 100 realizations in units of biomass (kg) and also approximated for C (biomass * 0.5).

2.9. Lidar-Derived Juniper Tree Density

[21] A variable local maxima approach [*Popescu and Wynne*, 2004] was used with the lidar point cloud data and lidar CHM to identify tree tops of the dominant canopy. Within each dominant tree, the lidar point cloud data across the voxel space was analyzed to identify subcanopy trees. When the distribution of aboveground height of lidar points showed multiple peaks at lower canopy levels, a horizontal window was moved downwards from the top to the bottom of each tree at a 1 m interval, and maxima was identified at every level. Overlapping maxima were later merged into a single tree top. All identified tree tops were then counted within 30 × 30 m cells. These estimates were regressed with field-based juniper density estimates in 30 × 30 m plots via a linear regression. The regression model was used to produce

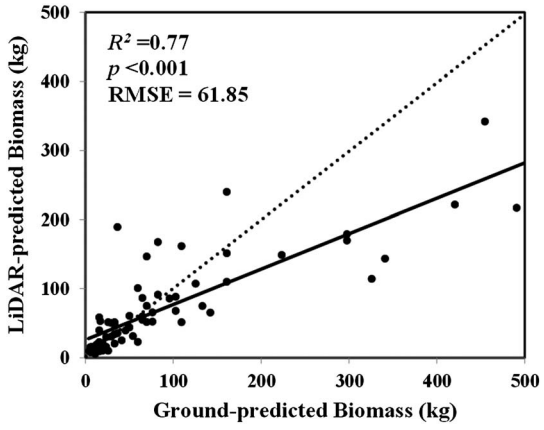

Figure 3. Relationship between lidar-predicted and observed juniper tree biomass.

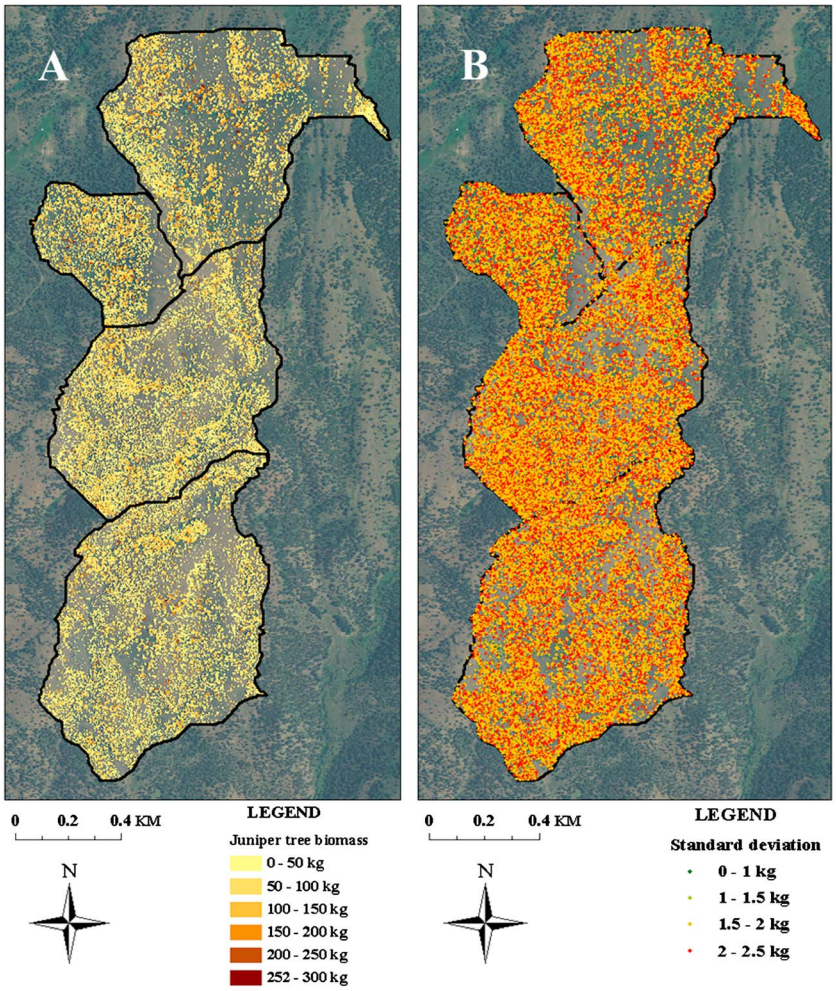

Figure 4. Juniper tree biomass in the South Mountain watershed study area. A total of 60,628 individual juniper trees were identified and their aboveground biomass estimated using lidar point cloud data (a). Uncertainty in the individual tree biomass estimates were then quantified using a Monte Carlo approach (b).

a lidar-derived juniper tree density map of the study area in 30 m cells.

2.10. Lidar-Derived Juniper Canopy Cover

[22] The vegetation point cloud data were converted into a raster format to estimate juniper tree canopy cover in 30 × 30 m cells. To generate this map, the vegetation point cloud data were first rasterized into 3 × 3 m cells using maximum vegetation height, so a total of 100 cells fell within each 30 × 30 cells thereby directly translating to a percent estimate comparable to the field measurement in the 30 m plots. A simple linear regression was performed to correlate the lidar-derived and field-measured individual juniper tree heights [SPSS 14.0 for Windows, 2005]. The regression model was used to produce a maximum tree height map across the study area in 3 m cells. A vegetation height binary map with a 3 m height threshold was then produced from the maximum vegetation height map. In the binary map, all pixels having maximum vegetation

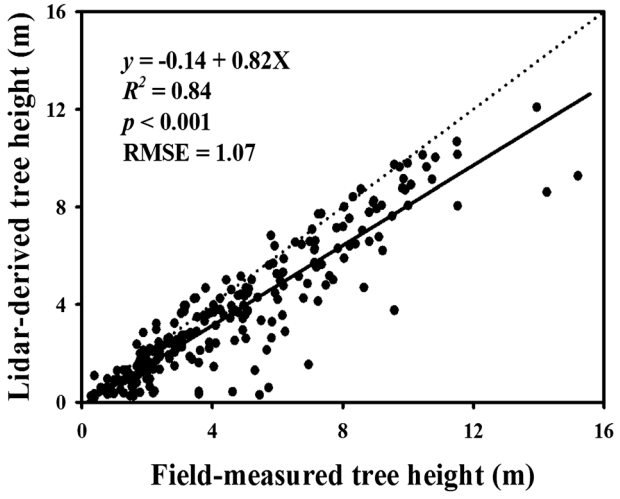

Figure 5. Relationship between field-measured and lidar-derived individual juniper tree heights.

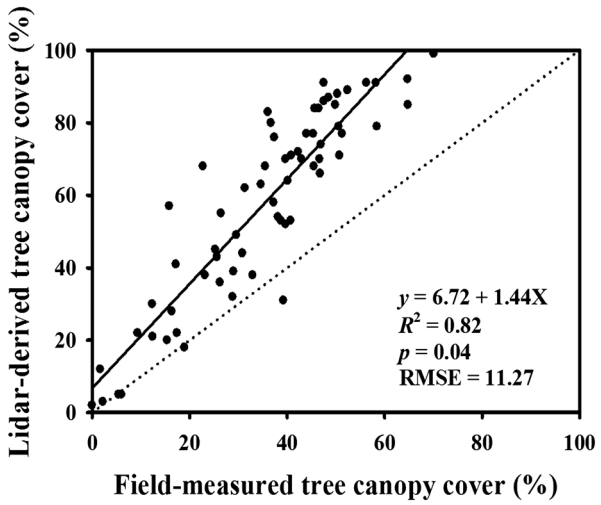

Figure 6. Relationship between field-measured [30 × 30 m plots] and lidar-derived [30 × 30 m cells] juniper tree canopy cover.

height >3 m were classified as juniper presence, while all other pixels were classified as juniper absence. This height threshold was chosen to best separate juniper trees from shrubs following *Sankey et al*. [2010]. A grid of 30 × 30 m cells of the study area was overlaid on the 3 m resolution binary height map and the number and percent of the 3 m pixels classified as having juniper presence within each 30 × 30 m cell was calculated to estimate juniper canopy percent cover. These estimates were regressed with the field-based juniper canopy cover estimates in 30 × 30 m plots via a linear regression. The regression model was used to produce a juniper canopy cover map of the study area in 30 m cells.

2.11. Lidar-Derived Classification of Juniper Encroachment Phases

[23] The lidar-derived canopy cover map was used to classify juniper encroachment phases across the watershed using phase thresholds suggested by *Miller et al*. [2005]. All pixels having <10% juniper cover were classified as encroachment phase I, while pixels with 10–30% and >30% were classified as encroachment phases II and III, respectively (Table 1). The lidar-derived canopy cover map was also used to classify encroachment phases using *Miller et al*. [2000] thresholds (<10%, 10–49%, and >49% for encroachment phases I–III, respectively).

[24] The lidar-derived tree density map was used to classify juniper encroachment phases across the watershed. All pixels having <18 trees (<200 trees/ha) were classified as encroachment phase I, while pixels with 18–70 trees (200–780 trees/ha) and >70 trees were classified as encroachment phases II and III, respectively (Table 1).

[25] The lidar-derived juniper phase maps derived from canopy cover and density thresholds were combined in ArcMap 9.3 to produce a final map of encroachment phase across the study area. All pixels classified into the same encroachment phase in both of the individual classifications remained the same. Any pixels that were classified in more than one phase were assigned the lower phase classification since they satisfied only one of the two criteria (e.g., cover or density).

3. Results

3.1. Field Measurements

[26] A total of 2613 juniper stems were mapped in 85 plots. Based on height, 554 of these stems were classified as seedlings and 2059 as mature trees. Mean juniper stem density was 288 stems/ha. Mean mature tree height was 7.3 m, and mean mature tree age was 72 years (Figure 2). Mean seedling height was 1.2 m, and mean seedling age was 48 years. Juniper tree age and height were significantly correlated (Adj. $R^2 = 0.48$, $p < 0.001$, RMSE = 23.63 years). However, given the relatively low coefficient of determination of 0.48, juniper tree age was not predicted across the watershed from lidar-derived height estimates.

3.2. Lidar Point Cloud Measurements

[27] The crown delineation approach identified 60,628 individual juniper trees across the study area. The best aboveground biomass model, which produced an adjusted R^2 value of 0.76 (Adj. $R^2 = 0.76$, $p < 0.001$, RMSE = 0.58 kg) (Figure 3), was

$$TB = 0.15 + 0.46CA + 0.31VHSS \quad (1)$$

where TB is the natural log-transformed total biomass, CA is the natural log-transformed crown area, and VHS is the natural log-transformed vegetation height sum of squares. The leave-one-out cross-validation R^2 of the model was 0.75. The estimate of mean aboveground tree biomass from this model was 45.5 kg (standard deviation ±34.8 kg). The total aboveground woody biomass in the watershed was 2760 Mg. The mean aboveground woody biomass was 13.5 Mg/ha, and the estimated mean aboveground woody C storage was 6.77 Mg/ha. Mean aboveground woody biomass in phases I, II, and III were 8.5, 18.9, and 23.1 Mg/ha, respectively.

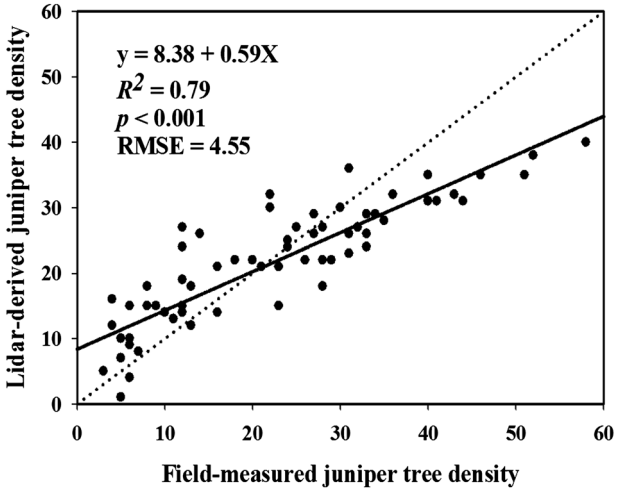

Figure 7. Relationship between lidar-derived [30 × 30 m cells] and field-measured [30 × 30 m plots] juniper tree density.

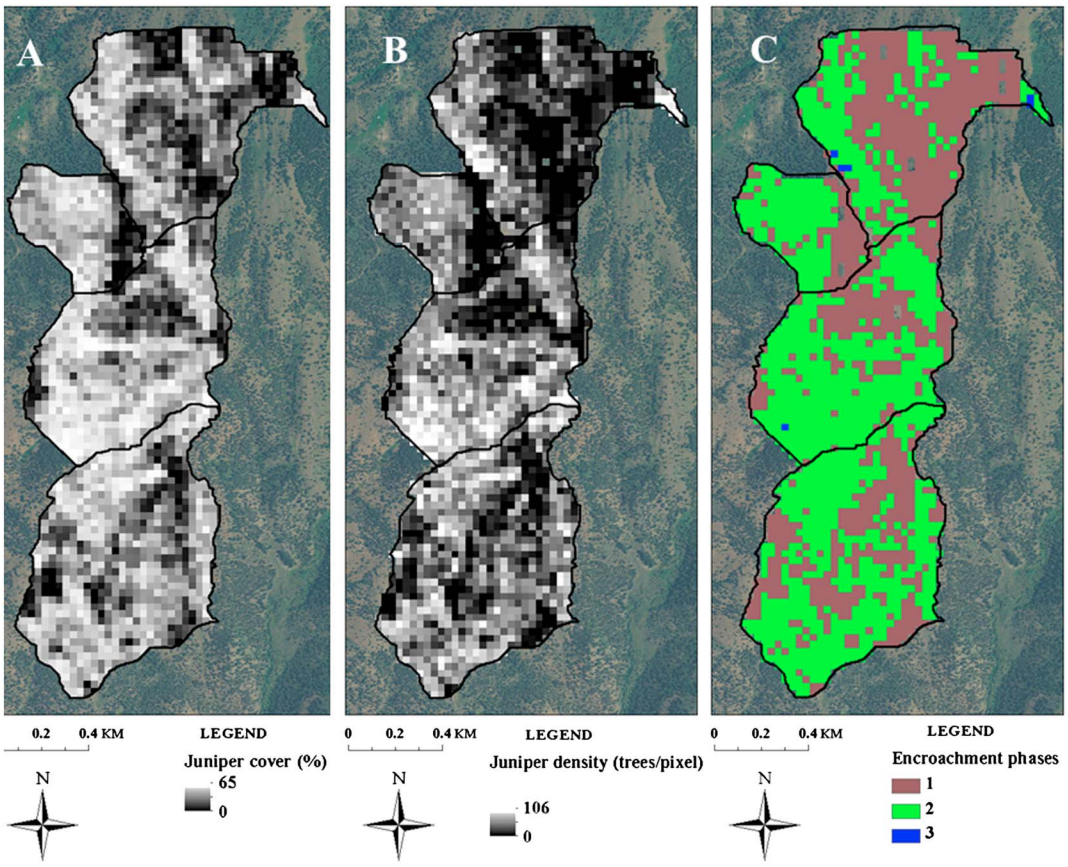

Figure 8. Lidar-predicted juniper canopy cover estimates in 30 × 30 m cells (a), lidar-predicted juniper tree density in 30 × 30 m cells (b), and final encroachment phase classification based on both juniper canopy cover and density estimates in 30 × 30 m cells (c).

3.3. Uncertainty

[28] The median of the 100 regression equations for field-based individual tree biomass as a function of the VHSS and CA lidar variables was:

$$TB = 0.36 + 0.42CA + 0.30VHSS \quad (2)$$

where TB is the natural log-transformed total biomass, CA is the natural log-transformed crown area, and VHSS is the natural log-transformed vegetation height sum of squares ($R^2 = 0.72$, $p < 0.001$, RMSE = 0.63 kg). The aboveground biomass of all individual trees delineated across the study area and determined for equation (2) is presented in Figure 4A. When the uncertainties in these estimates were examined using the Monte Carlo simulation of all four major error sources, the range in the predicted mean individual tree biomass and associated uncertainty (standard deviation) were 0.7 – 287.2 kg and 1.0 – 2.5 kg, respectively, for the entire study area (Figures 4A and 4B). These translate to C ranges of 0.35 – 143.6 kg and 0.5 – 1.25 kg, respectively. Visual examination of the map in Figures 4A and 4B indicates larger values of predicted biomass in areas of higher juniper density and later encroachment phases. The ranges in uncertainty (standard deviation) associated with individual tree biomass predictions from the Monte Carlo simulation were 1.1–2.4 kg, 1.0–2.5 kg, and 1.5–2.3 kg for encroachment phases 1–3, respectively. When the range in standard deviation for individual tree C estimates (0.5 – 1.25 kg) is extrapolated to the entire study area (60,628 trees within ~92 ha), an estimated range in uncertainty produced for C storage estimates is 0.16 – 0.40 Mg C/ha.

3.4. Lidar Raster Measurements

[29] Lidar-derived juniper tree heights were strongly correlated with field measurements (Adj. $R^2 = 0.84$, $p < 0.001$, RMSE = 1.07 m) (Figure 5). Lidar-derived juniper tree canopy cover in 30 × 30 m cells was strongly correlated with field-measured tree canopy cover in 30 m plots (Adj. $R^2 = 0.82$, $p = 0.04$, RMSE = 11.27%) (Figure 6). A juniper tree canopy cover map of the study area is presented in Figure 8A. When successional phases of juniper encroachment were classified based on the lidar-predicted juniper tree canopy cover and *Miller et al.* [2005] thresholds, 12% of the watershed was classified as phase I, 23% as phase II, and 65% as phase III. When *Miller et al.* [2000] thresholds were used instead, 12% were classified as phase I, 60% as phase II, and 28% as phase III.

[30] Lidar-derived and field-measured juniper tree density estimates were also strongly correlated (Adj. $R^2 = 0.79$, $p < 0.001$, RMSE = 4.55 trees/pixel) (Figure 7). A juniper tree density map of the study area is presented in Figure 8B. In the density-based classification model, 43% of the watershed was classified as phase I, 57% as phase II, and only 0.3% as phase III. In the fusion model that combined density thresholds with *Miller et al.* [2005] cover thresholds

(Figure 8C), 10%, 89.7%, and 0.3% of the watershed were classified as phases I–III, respectively.

4. Discussion

4.1. South Mountain Juniper Communities

[31] Field-measured tree-age data indicate that the western juniper communities in the study area are characteristic of postsettlement expansion communities [*Miller and Wigand*, 1994; *Miller et al*., 2005]. The juniper tree-age distribution in this study included very few trees established prior to 1850 (Figure 2). *Johnson and Miller* [2006] indicate that western juniper encroachment rates increase as trees reach maximal reproductive maturity at 50–70 years of age [*Miller and Rose*, 1995]. The mean mature tree age of 72 years in the study area might, therefore, indicate that the juniper communities are at a critical morphological stage. In the coming decades, juniper management could become increasingly difficult in these watersheds because encroachment rates would be expected to continue to increase, while control treatments might become less effective [*Tausch et al*., 1981, *Miller et al*., 2000, *Johnson and Miller*, 2006].

[32] Tree age was significantly correlated with height, but the relationship was relatively weak ($R^2 = 0.48$) most likely due to the large variability in height of older trees [e.g., >80 years old; *Miller et al*., 2005]. Previous studies indicate that the growth of western juniper trees in height is relatively slow at 30–40 mm yr^{-1} for the first 10 years, but increases to 90–170 mm yr^{-1} for older trees [*Miller et al*., 2005]. Western juniper tree canopy height reaches its maximum at approximately 80 years of age and maximum heights can range between 6 and 15 m [*Miller et al*., 2005]. The relatively low mature tree heights (mean = 7.3 m) observed in the study area might indicate that many of the trees have not reached their potential maximum heights. Lidar-derived juniper tree heights provide information on the spatial variability of active canopy growth.

4.2. Carbon Stocks in Juniper Woodlands

[33] Our results indicate that lidar-derived, three-dimensional measurements provide accurate estimates of aboveground woody C. The estimated mean aboveground woody biomass in this study was 13.5 Mg/ha. *Huang et al*. [2009] estimated aboveground woody biomass of 10.9 Mg/ha using Landsat ETM + data and indicated that the estimate was significantly lower than field-based estimates. *Huang et al*. [2009] also estimated aboveground woody biomass of 17.3 Mg/ha using higher-resolution AVIRIS data, which they documented to have better correlation with field-based juniper cover measurements than Landsat ETM+. *Strand et al*. [2008] further illustrated the need for high-resolution C estimates at regional scales by documenting that the difference between C accumulation rates estimated with coarse versus fine spatial resolution data ranged between 3.3 and 22 g C/m^2/year for western juniper in Idaho as well as 1.9 and 50 g C/m^2/year for mesquite in Texas, and 16.9 and 180 g C/m^2/year for oak savanna in Minnesota.

[34] Lidar-derived juniper canopy cover had a stronger correlation with field measurements compared to previous two-dimensional measurements using aerial photography and Landsat ETM + [*Strand et al*., 2008, *Huang et al*., 2009]. Lidar-derived versus field-based estimates of juniper cover in this study had a correlation coefficient of 0.82 with estimated error [RMSE] of 11%, while *Strand et al*. [2008] documented correlation coefficients of 0.60 and 0.74 with error [RMSE] of 13% and 27%, respectively, using wavelet and texture analyses. However, *Strand et al*. [2008] found smaller errors in their individual crown diameter estimates [RMSE = 2.60 m in crown diameter versus RMSE = 10.07 m in crown area in this study], and *Huang et al*. [2009] reported a stronger correlation, though no RMSE was reported, between their AVIRIS-based and field-based canopy cover estimates [$R^2 = 0.92$]. The integration of lidar-derived height of individual juniper trees might have contributed to the strong correlation [$R^2 = 0.77$] with observed aboveground woody biomass in our study. *Huang et al*. [2009] documented R^2 of 0.52 when correlating Landsat ETM + estimates with observed aboveground woody biomass and suggested that the uncertainties in C estimates could be reduced by using lidar data and integrating juniper height, which they hypothesized would be strongly correlated with aboveground woody biomass.

[35] The observed errors in our estimates might be due to the vegetation characteristics and plot sizes (*Zolkos et al*., 2013). Additional errors might have been introduced due to the characteristics of the lidar system used including sampling density, footprint size, and the digitization interval of return pulses. Most small-footprint systems such as the one used in this study typically have a footprint size of up to 50 cm, which lends itself to undersampling the vegetation canopy tops and hence underestimating the vegetation height [*Dubayah and Drake*, 2000; *Nelson*, 1997]. Furthermore, discretization interval in discrete return systems is usually around 2–3 m, which limits the vertical discrimination distance (the Leica ALS50 used in the study has an interval of 2.8 m [*Leica*, 2013]). In the future, some of the errors attributed to lidar systems may be minimized as airborne systems with higher point density and full-waveform capability become widely available. Also, with the advancements in multisensor fusion technology, the inherent limitations of lidar systems can be mitigated by using lidar data in synergy with other sensors (e.g., hyperspectral).

[36] The estimated aboveground woody C storage in our study supports previous conclusions that woody encroachment can increase the aboveground C sink [*Pacala and Hurtt*, 2001]. Juniper encroachment has been documented to lead to loss of understory sagebrush cover in the Great Basin [*Miller et al*., 2000]. In intact sagebrush shrublands that are not invaded by juniper, aboveground C storage in plant biomass has been estimated at 250–650 gC/m^2 by several studies [*Bradley et al*., 2006; *Hooker et al*., 2008; *Cleary et al*., 2008, 2010]. Based on an approximate average of 450 gC/m^2 from these studies, and the mean western juniper aboveground woody C estimate of 677 gC/m^2 (with an uncertainty estimate in the range of 16 – 40 gC/m^2 derived from standard deviations estimated for individual tree biomass calculations) from our study, we estimate that juniper encroachment might lead to an average increase in aboveground C of 227 gC/m^2. As sagebrush steppe vegetation is eventually replaced by juniper, the average increase in aboveground C would be 2.27 MgC/ha across the landscape. At a broader scale, this might translate to a total C sink of

27,559,092 MgC across the entire juniper woodland distribution of 12,140,569 ha in the United States when assuming a complete shift from sagebrush steppe vegetation to juniper woodlands.

[37] *Strand et al*. [2008] estimated belowground C stocks in juniper woodlands from aboveground biomass using a factor of 0.25. While belowground carbon estimate was not our objective in this study, we cautiously use this factor as a general guideline to approximately estimate belowground carbon. We estimate that the increase in the aboveground C sink that might occur with a complete shift from sagebrush steppe vegetation to juniper woodlands would translate to an additional 13,779,545 MgC belowground across the entire distribution of sagebrush communities in the USA. However, this does not account for the relatively large belowground C storage capacity of sagebrush steppe that has been estimated at 20 Mg/ha by one previous study [*Rau et al*., 2009]. This suggests that the increase in aboveground C storage might not offset the changes to belowground C that can occur from the conversion of sagebrush shrublands to juniper woodlands. Furthermore, the impact of woody encroachment on soil C pools so far has been controversial as some studies have shown an increase in soil C following woody plant encroachment [*Harrington and Williams*, 2008; *Reiley*, 2003; *Conant et al*., 1998; *Krammer and Green*, 2000; *Liao et al*., 2006; *Neff et al*., 2009], while others have found soil C stocks to either decrease or have a more complex response that varies nonlinearly by encroachment phase [*Rau et al*., 2011; *Jackson et al*., 2000]. Clearly, an integrated approach that simultaneously quantifies changes, and associated uncertainties, in both above- and belowground C pools is necessary for future research to determine whether juniper encroachment leads to a net C sink or source.

4.3. Lidar-Derived Variables

[38] Our results indicated that lidar-derived measurements produced accurate estimates of juniper tree height, canopy cover, and density. The strong relationships between lidar-derived and field-measured tree heights were similar to a previous lidar-based juniper study [*Sankey et al*., 2010]. However, tree heights appear to be underestimated especially for taller trees as the underestimation seem greater for these trees. Previous lidar studies have documented greater relative height error in trees compared to lower vegetation of herbaceous and shrub species [*Hopkinson et al*., 2004]. Previous studies have also documented underestimation of vegetation height with lidar [*Mitchell et al*., 2011; *Glenn et al*., 2011; *Sankey and Bond*, 2011] associated with laser pulse penetration into the vegetation canopy, low point density of the lidar data in the upper canopy portions that potentially miss the canopy top [*Gaveau and Hill*, 2003], and overestimation of ground height in densely vegetated areas that prevents laser pulse penetration [*Hopkinson et al*., 2004; *Gould et al*., 2013].

[39] The lidar-derived canopy cover was significantly and strongly correlated with field-measured canopy cover resulting in an R^2 of 0.82, which is greater than previous juniper cover estimates based on lidar data ($R^2 = 0.74$ in *Sankey and Glenn* [2011]; $R^2 = 0.69$ in *Sankey et al*., 2010]). Lidar, however, tended to overestimate juniper canopy cover, which was evidenced by both the steep slope and relatively large intercept of the regression line relating lidar-derived and field-measured canopy cover (Figure 6). Overestimation was greater when smaller height thresholds of 1 m and 2 m were used. Consistent with a previous finding [*Sankey et al*., 2010], the 3 m height threshold appeared most appropriate as it produced a similar coefficient of determination, but smaller regression intercept and slope coefficients compared to the lower (1 and 2 m) height thresholds. The observed overestimation might be due to the 3 × 3 m cells, in which juniper presence/absence was determined. Trees that are in reality smaller than 3 × 3 m in canopy diameter were assumed to take up the entire 3 × 3 m pixels. Smaller pixel sizes might be considered and tested for more accurate canopy cover prediction.

4.4. Classification of Encroachment Phases

[40] The encroachment phase classification results varied greatly depending upon the lidar variable used as well as the cover thresholds used. The first juniper cover-based classification indicated that 63% of the area was in encroachment phase III (>30% canopy cover) whereas 12% was in encroachment phase I (<10% cover). *Miller et al*. [2005] recommended these canopy cover thresholds as characteristics that can be used regardless of plant association or site potential. In contrast, when tree density thresholds were used, only 0.3% of the watershed was classified as encroachment phase III, and an overwhelming majority of the watershed was classified as encroachment phases I and II [43% and 57%, respectively]. Tree density thresholds in this study were based on *Johnson and Miller's* [2006] modeled estimates of tree density on varying topographic positions in the three encroachment phases. Given these large inconsistencies and commonly used land management practices that consider both juniper cover and density, it was important to integrate both variables. When we combined the lidar-derived cover and density estimates in the fusion model, a majority of the pixels met only one of the two criteria used (e.g., cover or density threshold) and were classified as encroachment phases I and II. Tree density was generally much lower in the study area (mean = 288 trees/ha) compared to that modeled in *Johnson and Miller* [2006]. Juniper canopy cover instead might be a more useful variable due to its variability across the watershed. In using canopy cover alone as a key criterion, the thresholds defined by *Miller et al*. [2000] might provide better guidelines than the *Miller et al*. [2005] thresholds since the observed variability in juniper cover is more consistent with the ranges found in the former. Furthermore, our field observation and local knowledge of the area do not support the finding that a large majority of the watershed is in encroachment phase III as would be indicated when using the approach of *Miller et al*. [2005]. Taken together, our results indicate that managers interested in accurately identifying encroachment phases might have to carefully consider whether to base the classification on juniper canopy cover or density.

[41] The thresholds defined in previous studies were intended to help identify windows of opportunity for efficient juniper control before reaching the phase III stage [*Johnson and Miller*, 2006]. Federal land management agencies now regularly perform intensive land treatments to reduce juniper cover and density [*Miller et al*., 2005]. These treatments include prescribed burning, cutting, and

mechanical shredding of trees [*Cline et al*., 2010]. Treatment effectiveness, however, varies as a function of encroachment phase [*Cline et al*., 2010]. Treatments are most effective during the early stages of stand development [*Miller et al*., 2000] and can be much more expensive and less effective for encroachment phase III [*Johnson and Miller*, 2006]. As juniper trees mature and canopies close during phase III, understory sagebrush and herbaceous cover drastically decline [*Blackburn and Tueller*, 1970; *Tausch et al*., 1981; *Miller et al*., 2000; *Waichler et al*., 2001] leading to soil exposure and increased probabilities of erosion [*Pierson et al*., 2010]. Re-establishment of herbaceous and shrub species after juniper removal can be compromised if soil organic matter and nutrients were lost to erosion in phase III conditions [*Cline et al*., 2010].

5. Conclusions and Management Implications

[42] Our results indicated that aboveground C storage is enhanced during the transition from phase I to phase III of successional stages of juniper encroachment. Phase III can store almost three times the aboveground C as encroachment phase I. While the net effect of encroachment on combined above- and belowground C storage is unclear and likely varies with the composition of the previous vegetation community, intensive juniper treatment activities that are commonly employed to counteract woody encroachment can potentially have long-lasting influences on C dynamics. Prescribed burning, cutting, and mechanical shredding are common intensive treatments that specifically result in an immediate and significant decline in aboveground C. Increased restoration challenges and unpredictable treatment effects are especially prevalent in the later stages of encroachment. We suggest that prioritizing locations in the earlier stages of encroachment for intensive treatment might strike a better balance between the success of management treatments on the one hand, and C storage goals on the other, over geographically extensive areas. Land managers might be better able to effectively maintain desired shrub steppe or grassland vegetation communities and have a less detrimental impact on C storage by focusing intensive treatment in phase I. It is important to acknowledge, however, that impacts of treatment activities such as overstory vegetation removal and prescribed fire on many ecosystem C processes, and especially belowground soil processes, are uncertain. We, therefore, recommend techniques that combine an improved understanding of belowground effects of management treatments with accurate estimates of aboveground biomass and C over large geographic areas using a three-dimensional approach such as illustrated here.

[43] **Acknowledgments.** This research was funded by Grant NA05OAR4601137 from the NOAA Earth System Research Laboratory Physical Sciences Division and the BLM Owyhee Uplands Pilot Project [ISU-BLM Agreement #DLA060249; and ARS-BLM Agreement #DLI050018]. This study was also supported by the NSF Idaho EPSCoR Program and by the NSF under award number EPS-0814387 and CBET-0854553. The authors would like to thank the Stanford and Lowry families for allowing access to these watersheds for our field monitoring. USDA is an equal opportunity provider and employer. Mention of trade names or commercial products in this publication is solely for the purpose of providing specific information and does not imply recommendation or endorsement by the U.S. Geological Survey. This research was supported by a U.S. Geological Survey Mendenhall Fellowship, and the U.S. Geological Survey Land Remote Sensing Program (Joel Sankey).

References

Aalde, H., P. Gonzalez, M. Gytarsky, T. Krug, W. A. Kurz, and S. Ogle (2006), Forest land. Intergovernmental Panel on Climate Change, in *National Greenhouse Gas Inventory Guidelines*, *4*, 1–83, Institute for Global Environmental Strategies, Hayama, Japan.

Archer, S. (1999), Woody plant encroachment into southwestern grasslands and savannas: Rates, patterns and proximate causes, in *Ecological Implications of Livestock Herbivory in the West*, edited by M. Vavra, W. Laylock, and R. D. Pieper, pp. 13–69, Society for Range Management, Denver, CO.

Asner, G. P., et al. (2010), High-resolution forest carbon stocks and emissions in the Amazon, *Proc. Natl. Acad. Sci.*, *107*, 16,738–16,742.

Bates, J. D., K. W. Davies, and R. N. Sharp (2011), Shrub-steppe early succession following juniper cutting and prescribed fire, *Env. Manage*, *47*, 468–481.

Benz, U. C., P. Hoffmann, G. Willhauck, I. Lingenfelder, and M. Heynen (2004), Multi-resolution, object-oriented fuzzy analysis of remote sensing data for GIS-ready information, *ISPRS J. Photogr. Rem. Sens.*, *58*, 239–258.

Blackburn, W. H., and P. T. Tueller (1970), Pinyon and juniper invasion in black sagebrush communities in east-central Nevada, *Ecology*, *51*, 841–848.

Bork, E. W., and J. G. Su (2007), Integrating LiDAR data and multispectral imagery for enhanced classification of rangeland vegetation: A meta analysis, *Rem. Sens. Env.*, *111*, 11–24.

Bradley, B. A., R. A. Houghton, J. F. Mustard, and S. P. Hamburg (2006), Invasive grass reduces aboveground carbon stocks in shrublands of the western US, *Glob. Change Biol.*, *12*, 1815–1822.

Cleary, M. B., E. Pendell, and E. B. Ewers (2008), Testing sagebrush allometric relationships across three fire chronosequences in Wyoming, USA, *J. Arid Env.*, *72*, 285–301.

Cleary, M. B., E. Pendell, and E. B. Ewers (2010), Aboveground and belowground carbon pools after fire in mountain big sagebrush steppe, *Range. Ecol. Manage.*, *63*, 187–196.

Cline, N. L., B. Roundy, F. Pierson, P. Kormos, and J. Williams (2010), Hydrologic response to mechanical shredding in a juniper woodland, *Range. Ecol. Manage.*, *63*, 467–477.

Conant, R. T., J. M. Klopatek, R. C. Malin, and C. C. Klopatek (1998), Carbon pools and fluxes along an environmental gradient in northern Arizona, *Biogeochemistry*, *43*, 43–61.

Davies, K. W., and J. D. Bates (2010), Vegetation characteristics of mountain and Wyoming big sagebrush plant communities in the Northern Great Basin, *Range. Ecol. Manage.*, *63*, 461–466.

Dubayah, R. O., and J. B. Drake (2000), Lidar remote sensing for forestry, *J. For.*, *98*, 44–46.

Gaveau, D. L. A., and R. A. Hill (2003), Quantifying canopy height underestimation by laser pulse penetration in small-footprint airborne laser scanning data, *Can. J. Remote Sens.*, *29*, 650–657.

Gholz, H. L., C. C. Grier, A. G. Campbell, and A. T. Brown (1979), Equations for estimating biomass and leaf area of plants in the Pacific Northwest, *Ore. State Univ. For. Res. Lab. Res. Pap.*, 41, Corvallis, OR.

Glenn, N. F., L. Spaete, T. Sankey, D. Derryberry, S. Hardegree, and J. Mitchell (2011), Errors in LiDAR-derived shrub height and crown area on sloped terrain, *J. Arid Env.*, *75*(4), 377–382, doi:10.1016/j.jaridenv.2010.11.005.

Gonzalez, P., G. P. Asner, J. J. Battles, M. A. Lefsky, K. M. Waring, and M. Palace (2010), Forest carbon densities and uncertainties from Lidar, Quickbird, and field measurements in California, *Rem. Sens. Env.*, *114*, 1561–1575.

Gould, S., N. Glenn, T. Sankey, J. McNamara, and L. Spaete (2013), Influence of a dense, low-height shrub species on the accuracy of a LiDAR-derived DEM, *Photogram. Eng. Rem. Sens.*, *79*, 421–431.

Harrington, J., and M. Williams (2008), Belowground carbon distribution in a pinyon-juniper/short grass prairie site, in *Ecology, management, and restoration of pinon-juniper and ponderosa pine ecosystems: Combined proceedings of the 2005 St. George, Utah and 2006 Albuquerque, New Mexico workshops*, edited by G. J. Gottfried, J. D. Shaw, and P. L. Ford, Proc. RMRS-P-51.

Hocking, R. R. (2003), *Methods and applications of linear models: Regression and the analysis of variance*, John Wiley, Hoboken, N. J.

Hooker, T. D., J. M. Stark, N. A. Urszula, J. Leffler, M. Peek, and R. Ryel (2008), Distribution of ecosystem C and N within contrasting vegetation types in a semiarid rangeland in the Great Basin, USA, *Biogeochemistry*, *90*, 291–308.

Hopkinson, C., L. E. Chasmer, G. Zsigovics, I. F. Creed, M. Sitar, P. Treitz, and R. V. Maher (2004), Errors in LiDAR ground elevation and wetland vegetation height estimates, in *Laser-Scanners for Forest and Landscape Assessment*, Proc. ISPRS working group VIII/2, October 2004, ISPRS 36, PART 8/W2, Freiburg, Germany 03-06.

Houghton, R. A. (2003), Why are estimates of the terrestrial carbon balance so different?, *Glob. Change Biol.*, *9*, 500–509.

Houghton, R. A., J. L. Hackler, and K. T. Lawrence (1999), The US carbon budget: contributions from land-use change, *Science*, *285*, 574–578.

Huang, C., G. P. Asner, R. Martin, N. Barger, and J. Neff (2009), Multiscale analysis of tree cover and aboveground carbon stocks in pinyon–juniper woodlands. *Ecol. App.*, *19*, 668−681.

Hyyppa, J., O. Kelle, M. Lehikoinen, and M. Inkinen (2001), A segmentation-based method to retrieve stem volume estimates from 3-dimensional tree height models produced by laser scanner, *IEEE Trans. Geosci. Remote Sens.*, *39*, 969–975.

Jackson, R. B., et al. (2000), Belowground consequences of vegetation change and their treatment in models, *Ecol. App.*, *10*, 470–483.

Johnson, D., and R. F. Miller (2006), Structure and development of expanding western juniper woodlands as influenced by two topographic variables, *For. Ecol. Manage.*, *229*, 7–15.

Koch, B. (2010), Status and future of laser scanning, synthetic aperture radar and hyperspectral remote sensing data for forest biomass assessment, *ISPRS J. Photogramm.*, *65*, 581–590.

Krammer, S., and D. M. Green (2000), Acid and alkaline phosphate dynamics and their relationship to soil microclimate in a semiarid woodland, *Soil Biol. Biochem.*, *32*, 179–188.

Leica ALS50—Airborne Laser Scanner Product Specifications. [Online]. Available at: http://www.unicaen.fr/recherche/clarec/IMG/pdf/ALS50_brochure.pdf.

Liao, J. D., T. W. Boutton, and J. D. Jastrow (2006), Organic matter turnover in soil physical fractions following woody plant invasion of grassland: Evidence from natural 13C and 15N, *Soil Biolog. Biochem*, *38*, 3197–3210.

Mather, A. (2000), South–north challenges in global forestry, in *World Forests from Deforestation to Transition*, edited by M. Palo and H. Vananen, Kluwer Academic Publishers, Dordrecht.

Means, J. E., S. A. Acker, B. J. Fitt, M. Renslow, L. Emerson, and C. J. Hendrix (2000), Predicting forest stand characteristics with airborne scanning lidar, *Photogr. Eng. Rem. Sens*, *66*(11), 1367–1371.

Miller, R. F., and J. A. Rose (1995), Historic expansion of *Juniperus occidentalis* (western juniper) in southeastern Oregon, *J. Range Manage.*, *55*, 37–45.

Miller, R. F., and J. A. Rose (1999), Fire history and western juniper encroachment in sagebrush steppe, *J. Range Manage.*, *52*, 550–559.

Miller, R. F., and P. E. Wigand (1994), Holocene changes in semiarid pinyon-juniper woodlands, *Bioscience*, *44*, 465–473.

Miller, R. F., T. J. Svejcar, and J. A. Rose (2000), Impacts of western juniper on plant community composition and structure, *J. Range Manage.*, *53*, 574–585.

Miller, R. F., J. D. Bates, T. J. Svejcar, F. B. Pierson, L. E. Eddleman (2005), Biology, Ecology, and Management of Western Juniper (Juniperus occidentalis). Ore. State Univ. Agric. Exp. Sta. Tech. Bull. No. 152, 77 pp. Corvallis, OR.

Mitchell, J., N. F. Glenn, T. Sankey, D. R. Derryberry, M. O. Anderson, and R. Hruska (2011), Small-footprint LiDAR estimations of sagebrush canopy characteristics, *Photogr. Eng. Rem. Sens.*, *77*(5), 521–530.

Montgomery, D. C., E. A. Peck, and G. G. Vining (2006), *Introduction to linear regression analysis*, 4th ed., John Wiley, Hoboken, N. J.

Mundt, J. T., D. R. Streutker, and N. F. Glenn (2006), Mapping sagebrush distribution using fusion of hyperspectral and lidar classifications, *Photogr. Eng. Rem. Sens.*, *72*, 47–54.

Næsset, E., and T. Gobakken (2008), Estimation of above- and below-ground biomass across regions of the boreal forest zone using airborne laser, *Rem. Sens. Env.*, *112*(6), 3079–3090.

Neff, J. C., N. N. Barger, W. T. Baisden, D. P. Frenandez, and G. P. Asner (2009), Soil carbon storage responses to expanding pinyon–juniper populations in southern Utah, *Ecol. App.*, *19*, 1405–1416.

Nelson, R. (1997), Modeling forest canopy heights: The effects of canopy shape, *Rem. Sens. Env.*, *60*, 327–334.

Pacala, S. W., and G. C. Hurtt (2001), Consistent land- and atmosphere-based U.S. carbon sink estimates, *Science*, *292*, 2316–2319.

Pan, Y., et al. (2011), A large and persistent carbon sink in the world's forests, *Science*, doi:10.1126/science.1201609.

Pierson, F. B., C. J. Williams, P. R. Kormos, S. P. Hardegree, P. Clark, and B. M. Rau (2010), Hydrologic vulnerability of sagebrush steppe following pinyon and juniper encroachment, *Range. Ecol. Manage.*, *63*, 614–629.

Popescu, S. C. (2007), Estimating biomass of individual pine trees using airborne lidar, *Biomass Bioenergy*, *31*, 646–655.

Popescu, S. C., and R. H. Wynne (2004), Seeing the trees in the forest: Using lidar and multispectral data fusion with local filtering and variable window size for estimating tree height, *Photogr. Eng. Rem. Sens.*, *70*, 589–604.

Popescu, S. C., R. H. Wynne, and R. F. Nelson (2003), Measuring individual tree crown diameter with lidar and assessing its influence on estimating forest volume and biomass, *Can. J. Rem. Sens.*, *29*, 564–577.

Rango, A., M. J. Chopping, J. C. Ritchie, K. Havstad, W. Kustas, and T. Schmugge (2000), Morphological characteristics of shrub coppice dunes in desert grasslands of southern New Mexico derived from scanning LiDAR, *Rem. Sens. Env.*, *76*, 26–44.

Rau, B. M., D. W. Johnson, R. R. Blank, and J. C. Chambers (2009), Soil carbon and nitrogen in a Great Basin pinyon–juniper woodland: Influence of vegetation, burning, and time, *J. Arid Env*, *73*, 472–479.

Rau, B. M., D. W. Johnson, R. R. Blank, R. J. Tausch, B. A. Roundy, R. F. Miller, T. G. Caldwell, and A. Lucchesi (2011), Woodland expansion's influence on belowground carbon and nitrogen in the Great Basin, U.S., *J. Arid Env*, *75*, 827–835.

Reiley, D. K. (2003), Land use history and effects on soil carbon storage patterns in a pinon-juniper woodland in northern New Mexico, MS thesis, Univ. of Wisc.-Madison, Madison.

Riano, D., E. Chuvieco, S. L. Ustin, J. Salas, J. R. Rodriguez-Perez, L. M. Ribeiro, D. Viegas, J. M. Moreno, and H. Fernandez (2007), Estimation of shrub height for fuel-type mapping combining airborne LiDAR and simultaneous color infrared ortho imaging, *Intern. J. Wildl. Fire*, *16*, 341–348.

Ritchie, J. C., K. S. Humes, and M. A. Weltz (1995), Laser altimeter measurements at Walnut Gulch watershed, Arizona, *J. Soil Wat. Cons.*, *50*, 440–442.

Romme, W. H., et al. (2009), Historical and modern disturbance regumes, stand structures, and landscape dynamics in pinon-juniper vegetation of the western United States, *Range. Ecol. Manage.*, *62*, 203–222.

Rozeboom, W. W. (1978), Estimation of cross-validated multiple correlation: A clarification, *Psych. Bull.*, *85*, 1348–1351.

Sankey, T. T., and P. Bond (2011), LiDAR-based classification of sagebrush community types, *Range. Ecol. Manage.*, *64*, 92–98.

Sankey, T., and M. Germino (2008), Assessment of juniper encroachment with the use of satellite imagery and geospatial data, *Range. Ecol. Manage.*, *61*, 412–418.

Sankey, T., and N. Glenn (2011), Landsat-5 TM and lidar fusion for sub-pixel juniper tree cover estimates in a western rangeland, *Photogr. Eng. Rem. Sens.*, *77*(12), 1241–1248.

Sankey, T. T., N. Glenn, S. Ehinger, A. Boehm, and S. Hardegree (2010), Characterizing western juniper expansion via a fusion of Landsat 5 Thematic Mapper and lidar data, *Range. Ecol. Manage.*, *63*, 514–523.

Stokes, M. A., and T. L. Smiley (1968), *An introduction to tree-ring dating*, Univ. of Chicago Press, Chicago, Ill.

Strand, E. K., L. A. Vierling, A. M. S. Smith, and S. C. Bunting (2008), Net changes in aboveground woody carbon stock in western juniper woodlands, 1946–1998, *J. Geophys. Res.*, *113*, G01013, doi:10.1029/2007JG000544.

Streutker, D. R., and N. F. Glenn (2006), LiDAR measurement of sagebrush steppe vegetation heights, *Rem. Sens. Env.*, *102*, 135–145.

Su, J. G., and E. W. Bork (2007), Characterization of diverse plant communities in Aspen Parkland rangeland using LiDAR data, *Appl. Veg. Sci.*, *10*, 407–416.

Tausch, R. J., N. E. West, and A. A. Nabi (1981), Tree age and dominance patterns in Great Basin pinyon-juniper woodlands, *J. Range Manage.*, *34*, 259–264.

Waichler, W. S., R. F. Miller, and P. S. Doescher (2001), Community characteristics of old-growth western juniper woodlands, *J. Range Manage.*, *54*, 518–527.

Wang, G., G. Z. Gertner, S. Fang, and A. B. Anderson (2005), A methodology for spatial uncertainty analysis of remote sensing and GIS products, *Photogramm. Eng. Rem. Sens.*, *71*, 1423–1432.

Weltz, M. A., J. C. Ritchie, and H. D. Fox (1994), Comparison of laser and field measurements of vegetation height and canopy cover, *Water Resour. Res.*, *30*, 1311–1319.

Zolkos, S. G., S. J. Goetz, and R. Dubayah (2013), A meta-analysis of terrestrial aboveground biomass estimation using lidar remote sensing, *Rem. Sens. Env.*, *128*, 289–298.